PHILOSOPHICAL TRANSACTIONS OF THE ROYAL SOCIETY B BIOLOGICAL SCIENCES

In vivo n.m.r. Imaging in Medicine: The Aberdeen Approach, both Physical and Biological [and Discussion]

J. Mallard, J. M. S. Hutchison, W. A. Edelstein, C. R. Ling, M. A. Foster, G. Johnson, S. F. J. Cox, P. C. Lauterbur, P. Mansfield, D. R. Wilkie and W. S. Moore

Phil. Trans. R. Soc. Lond. B 1980 **289**, 519-530
doi: 10.1098/rstb.1980.0071

Phil. Trans. R. Soc. Lond. B **289**, 519–533 (1980) [519]
Printed in Great Britain

In vivo n.m.r. imaging in medicine: the Aberdeen approach, both physical and biological

By J. Mallard, J. M. S. Hutchison, W. A. Edelstein, C. R. Ling, M. A. Foster and G. Johnson
Department of Bio-Medical Physics and Bio-Engineering, The University, Aberdeen, U.K.

[Plates 1–3]

A novel magnetic field and radio frequency (1.7 MHz) pulse sequence is described for a whole body n.m.r. imaging machine under construction. Selective excitation is used to obtain signals from successive lines of proton spins (water) across the body to build up an image of a transverse section. The images display spin concentration and spin–lattice relaxation time, T_1, separately. For a 50% change in T_1 to be discerned in the human trunk, a spatial resolution of 2 cm^3 is expected for a 2 min scan and 0.5 cm^3 for a 30 min scan. Very preliminary images at the present incomplete stage of development show the geometrical accuracy and T_1 discrimination: an *in vivo* image demonstrates some of the difficulties to be overcome.

In vitro measurements of normal rabbit tissue samples have been made at 24 MHz to map the T_1 distributions that can be expected from normal subjects. The transposition of this information from rabbit to man, and from 24 MHz to 2.5 MHz have been checked and the comparison shown to be meaningful. Of pathological samples, human breast tumour and human liver metastases offer a good contrast to their surrounding tissue, and an experimental investigation has shown that tissue immediately surrounding a tumour also has an elevated T_1 value. A wide range of abnormalities that are associated with abnormal fluid formation in the body may be amenable to imaging by the n.m.r. technique. Potential hazards are believed to be small in the present generation of equipment.

1. Introduction

The previous papers of this Discussion meeting have dealt with the principles of n.m.r. imaging and many of the techniques that are being used and the problems being encountered. These techniques have been reviewed by Hutchison (1979) and the Aberdeen n.m.r. imaging programme, both physical and biological, has been outlined by Mallard (1979) and Mallard *et al.* (1979).

Our programme in Aberdeen includes the building of a whole body n.m.r. imaging machine to produce transverse section distributions of the hydrogen proton spin–lattice relaxation time of water separately from the distribution of water proton concentration. Also, we have carried out *in vitro* measurements of spin–lattice relaxation time, T_1, of an extensive series of biological tissue samples. The results of these measurements provide a basis to predict imaging performance and, ultimately, a better understanding of features depicted.

2. Early images by reconstructed projections

Figure 1, plate 1, is a relaxation time image of a mouse, taken in Aberdeen in 1974 by means of an early n.m.r. imaging machine (Hutchison *et al.* 1974; Hutchison 1976). Twenty-five profiles were taken at different angles around the mouse and digitally reconstructed to form the

image. The proton concentration image was not particularly interesting except that it gave the outline of the animal, but the colours shown are coded by the relaxation time averaged through the whole thickness of the animal; this image is not a true tomograph but a dorsal projection. The yellow areas are the short T_1, and coincide with the expected position of the liver and other abdominal organs, which are known to have short T_1 values. The blue area, of longer T_1, is brain tissue, but the blue–black region, of very long T_1, near the neck is the exciting part of the picture. To make this crude image, the animal had to be completely still for about an hour. Immediately before the experiment, therefore, it was killed by breaking its neck. The region of long T_1 shows the fluid accumulation around the fracture. This very early whole animal n.m.r. image has shown pathological wound oedema, which has encouraged us to pursue the technique and to attempt to go straight from mouse to man.

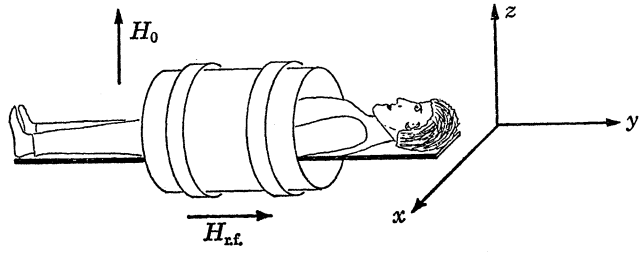

FIGURE 2. The relation between x, y, and z coordinates and the patient.

3. THE ABERDEEN WHOLE BODY IMAGING TECHNIQUE†

(*a*) *Selective excitation*

The Aberdeen machine uses the principle of selective excitation (Hutchison 1976) already described in earlier papers of this meeting. The particular treatment of selective excitation proposed (Sutherland & Hutchison 1978) has several important advantages. It tolerates a much larger magnetic field non-uniformity than does the projection reconstruction method before information is lost. This loss is irretrievable in the projection method if the non-uniformity exceeds about 1% of the field difference across the gradient, but, with selective excitation, field distortions of up to 50% can be tolerated (Hutchison *et al.* 1978). The effects of such distortions on imaging information can be removed by running a uniform reference sample under the same

† The subject of patents (in Britain and other countries) registered by N.R.D.C.: British Patent nos 25899/78 and 40779/78.

DESCRIPTION OF PLATE 1

FIGURE 1. Very early (1974) n.m.r. image of mouse imaging pathology. The outline of the animal is displayed from proton concentration. Colour is coded with average T_1 through thickness of animal (dorsal projection). Yellow is short T_1 (≡ liver) and blue longer T_1 (≡ brain). Black is longest T_1 (≡ wound oedema around fractured neck).

FIGURE 8. (*a*) The variations of T_1 relaxation time in normal muscle underlying and extending beyond the implant of Yoshida sarcoma in rat thigh seen in (*b*).

FIGURE 9. (*a*) The n.m.r. image of a square array of identical bottles of copper sulphate solution (see text). (*b*) The n.m.r. images and line profiles of two boxes of copper sulphate solution, the left having a T_1 value twice that of the right. Upper, S_A; central, S_B; lower, T_1 (see text).

FIGURE 10. The first human image (March 1979). Thorax cross section of one of us (J.M.S.H.) (8 min scan, proton concentration). The lungs, heart and spine are of recognizable position, shape and size. The artefact bar across and beyond the trunk section is due to heart beat movements, a problem remaining to be overcome.

1

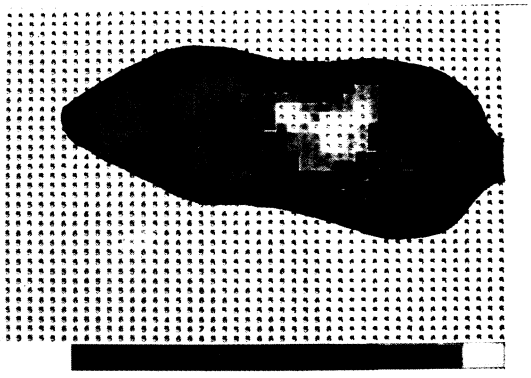

10

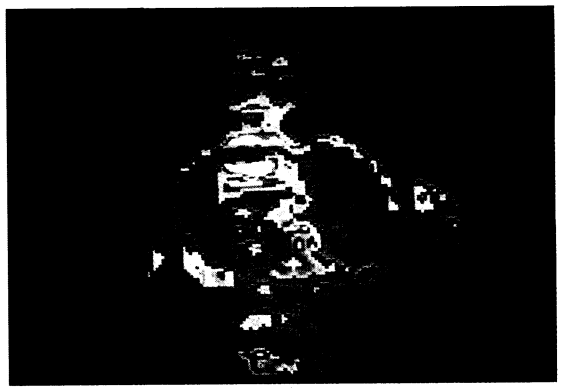

8a

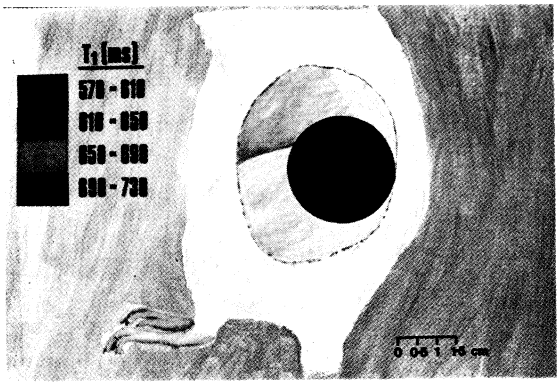

8b

9a

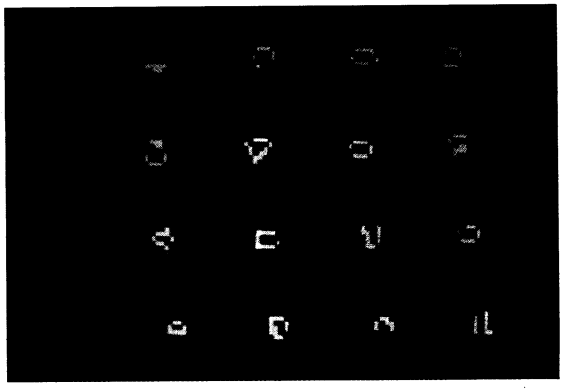

9b

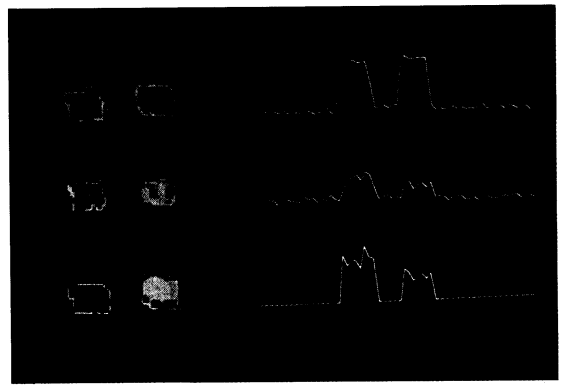

FIGURES 1, 8–10. For description see opposite.

PHILOSOPHICAL TRANSACTIONS OF THE ROYAL SOCIETY B BIOLOGICAL SCIENCES

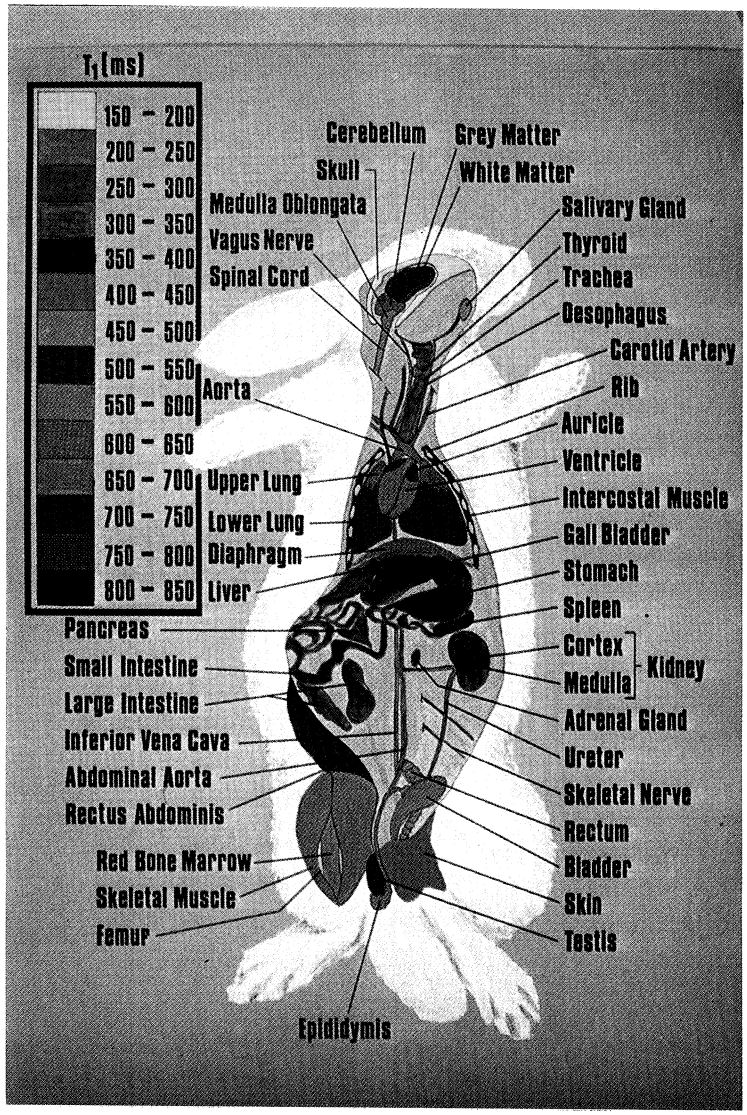

FIGURE 7. For description see opposite.

conditions as the unknown and using the signals from this to deconvolute those from the unknown sample. Also, each image line is independent. If the patient moves during one image line sequence, then only that line is upset, in contrast to the projection method, where the complete image frame is upset. In addition, it is not necessary to form a complete frame. One could, for example, run off a frame at course resolution, find an area of interest in it and then concentrate on a few lines in that area at finer resolution by means of signal averaging. Although, theoretically, in a perfectly uniform magnetic field, the projection reconstruction method gives a much higher signal : noise ratio, we believe that it is far more difficult to achieve when dealing with samples as large as the human trunk.

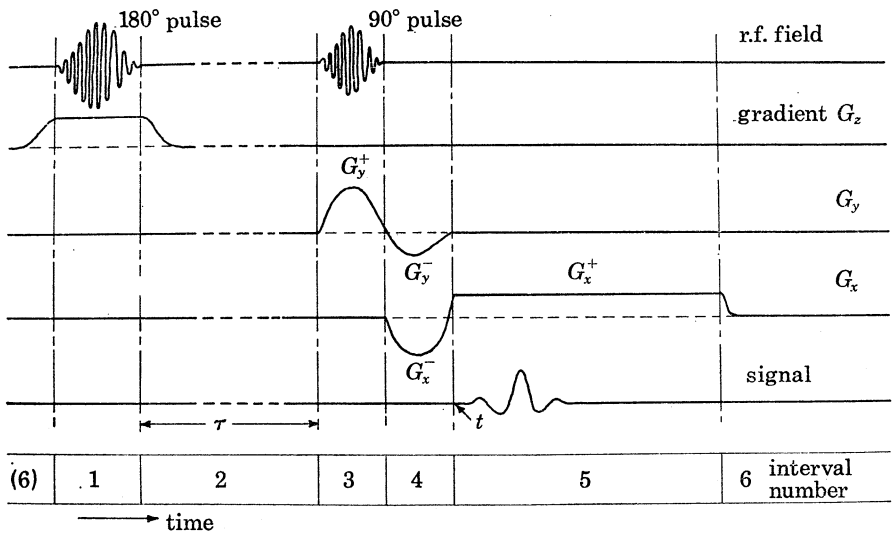

FIGURE 3. The main features (diagrammatic) of the r.f. pulse and magnetic field gradient basic sequence, divided into six intervals (not to scale).

While individual lines of spins are readily selected from a two-dimensional sample, this is not so for the third dimension. The technique described here overcomes this problem in a novel way, and the apparatus incorporates a number of other unique features.

Figure 2 relates x, y and z coordinates to the patient. The main magnetic field is in the z direction, from posterior to anterior, and the radio frequency field is in the y direction, along the long axis of the patient, who is supine. The selective excitation pulse sequence chooses a plane zx at $y = 0$, which is fixed on the machine, but can be changed relative to the patient by sliding him through the tube.

Figure 3 shows the main features of the r.f. pulse and magnetic field gradient sequence being used. It is divided into six intervals (not shown strictly to scale), of which intervals 3, 4 and 5 are the basic selection and observation sequence. Starting at interval 3 is the excitation of the line of spins across the patient (x) by application of a strong magnetic field gradient (G_y^+) in the

DESCRIPTION OF PLATE 2

FIGURE 7. Spin–lattice relaxation time of normal tissues of the rabbit drawn onto an antomical map of the rabbit, to illustrate the spatial disposition of the various T_1 values in the body (24 MHz).

y direction, at the same time as a 90° r.f. pulse. This combination gives the maximum transverse magnetization of the nuclear spins in the zx plane at $y = 0$. The r.f. carrier wave of this pulse is modulated to have a Gaussian amplitude wave form of 0.6 ms full width at half maximum (f.w.h.m.); this gives a Gaussian spectral profile of 1.8 kHz f.w.h.m. This shaping, together with the gradient G_y^+, defines the thickness of the transverse slice across the patient.

During the next interval, 4, these spins are deliberately brought into phase throughout this selected slice. This is achieved by application of an opposite negative field gradient pulse (G_y^-) of approximately half the size of the previous positive one (Sutherland & Hutchison 1978). At the same time, the spins are dephased along the x direction by application of another field gradient pulse (G_x^-) to prepare them for the main observation interval, 5. G_x is then driven to a constant positive value and the observation period begins at time t. During this observation interval, the spins rephase, producing a spin echo under the influence of the steady gradient G_x^+. The frequency of the spin echo from a particular spin packet is related to its position, x, in the strip across the patient.

None of the gradient waveforms have sharp edges. This is deliberate, to avoid excessive inductive potentials in the field gradient windings. G_y^+ is quite rounded, contrary to the usual practice when selective excitation is used. It is a half sine-function generated by discharging a bank of capacitors into the inductive gradient winding; and G_y^- is simply the next half-cycle continued, but suitably damped. This unusual combination has worked quite well.

The selection in the z direction has still to be explored. The strip at $z = z_1$ is excited by selectively inverting the spins that are in and close to the plane $z = z_1$ during interval 1 with a combination of a 180° r.f. pulse and another magnetic field gradient, G_z. This selectively inverts the spins, but only in the plane $z = z_1$, before the basic selection and observation sequence. The selection of the line is spoiled unless G_z is constant during the 180° r.f. pulse. To move to z_2, the carrier frequency used to generate the 180° pulse is shifted from the nominal central Larmor frequency by an increment. In practice, 2 kHz steps are used: the carrier frequency has 40 different values, each separated by 2 kHz, each one giving one line of the whole image, which is made up of 40 lines.

(*b*) *Separation of proton concentration and spin–lattice relaxation information*

The next part of the procedure is concerned with the way in which this basic pulse sequence, which is repeated once per second, is used to separate out two signals, one of which is related mainly to proton spin concentration and the other mainly to the spin–lattice relaxation time. This sequence is used in three different ways. First, the 180° pulse is omitted and hence there is no inversion and no selection in z. These signals are called S_0 signals; all S_0 signals are independent of T_1, but dependent upon the proton density, and are from the whole slice zx. Secondly, the interval 2, or the time τ, is made very short compared with any of the T_1 values being measured. In practice, τ is about 10 ms. These signals are called S_1. Thirdly, τ is made of comparable size to the T_1 values being measured, about 200 ms, and the signals are called S_2.

Two difference signals are then obtained:

$$S_A = S_0 - S_1 \quad \text{and} \quad S_B = S_0 - S_2.$$

S_A and S_B are Fourier transformed to provide the information for one image line: that derived from S_A contains data mainly related to spin density while that from S_B contains data mainly related to T_1.

PHILOSOPHICAL TRANSACTIONS OF THE ROYAL SOCIETY B BIOLOGICAL SCIENCES

Figure 4 shows how the parameters S_A and S_B depend on T_1. Values of S_A depend only slightly on T_1 and almost entirely on proton concentration, while S_B values are clearly releated to T_1. The dependence of S_B on T_1 can be optimized for a chosen range of T_1 values by adjusting the period of interval 2 to correspond with the range. The spread of S_B is shown for the various tissues that we have measured (see § 4 below). The two extremes of these graphs show an increasing uncertainty as T_1 becomes larger, which is due to the next sequence of pulses beginning before spins with long T_1 have fully relaxed.

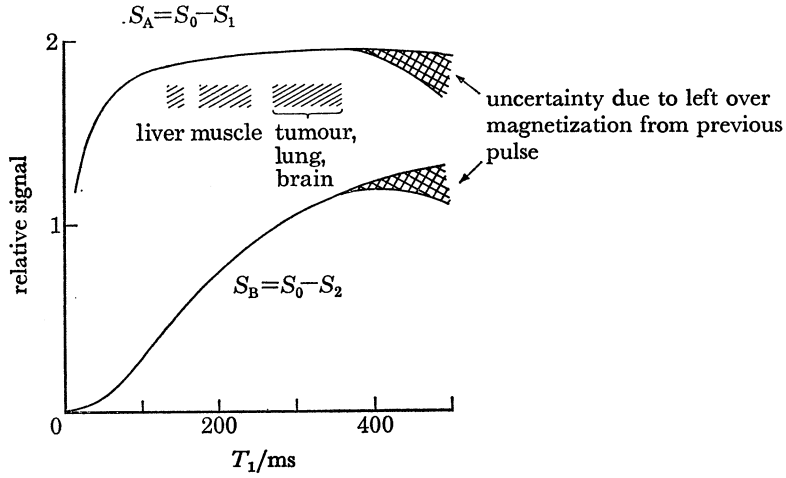

FIGURE 4. The dependence of S_A and S_B on T_1.

The signals S_0, S_1 and S_2 each take 1 s to obtain, 3 s for the complete set. As a result, one line of proton concentration information, and the same line of T_1 information, take 3 s. The 40-line image of a complete slice, containing both concentration and T_1 information, takes 120 s. It is the intention to relate the brightness of the display to S_A, which is mainly proton concentration, and the colour coding of the display to S_B, or T_1, and thereby display both, separately and simultaneously, but there are several other ways of arranging the display format.

(*c*) *The apparatus*

The apparatus is shown in figure 5, plate 3. The magnet is a four coil, air core electromagnet, which was the first one of its type built for human imaging†. It produces a static vertical field of 0.04 T, which corresponds to a proton n.m.r. frequency of 1.7 MHz. The power dissipation is 10 kW and a water cooling system is used.

In the figure, one of us (J.M.S.H.) is lying in the position of the patient inside a plastic tube of about 50 cm diameter. On the tube are wound the coils that produce the two field gradients across the patient, left to right and back to front. They are straight wires running along the cylindrical surface, with a winding density of cos 2θ and sin 2θ. They can easily be interchanged to give image lines running up and down instead of left to right. The G_z pulse is about 0.5 G/cm (5×10^{-3}T/m) to give image line spacing of one line per cm, which is the practical limit for the present design. The observation gradient, G_x, is about 0.05 G/cm (0.5×10^{-3}T/m, 200 Hz/cm). The windings also act as a Faraday shield for the radio frequency coil, which is wound outside and made of 8 mm copper tubing. They are two parallel coils operated in an electrically

† Oxford Instruments Ltd., Osney Mead, Oxford OX2 0DX, U.K.

PHILOSOPHICAL TRANSACTIONS OF THE ROYAL SOCIETY B BIOLOGICAL SCIENCES

balanced configuration which, in conjunction with the Faraday shield, gives virtually no electric field inside the cylinder. The unloaded Q (quality) factor is nearly 600, which drops only to 300 with the patient in position; this is a smaller drop than anticipated. The Q factor is damped still more by means of an active 'cold resistance' in the receiver, to avoid degradation of the signal/noise ratio.

The G_y windings are four external rectangular loops. A pulse of 40 A (up to 500 V) is needed to give the required field gradient of 0.5 G/cm (5×10^{-3} T/m); this is the reason for using the capacitor discharge system mentioned above. These windings select a plane (approximately 1 cm thick) across the patient.

The whole machine is contained in a non-magnetic, screened enclosure, about $2\frac{1}{2}$ m cubed, made of $\frac{1}{2}$ mm thick alumimium sheet, copper-nailed on a wooden frame and soldered next to the nailing points. This has successfully eliminated interference, which was 50 dB above the Johnson noise of the radio frequency coil. All power connections through the enclosure are fitted with electrical filters tuned to reject 1.7 MHz.

The n.m.r. induction signal at 1.7 MHz is amplified and fed to two balanced demodulators operating in phase quadrature, the two low frequency signals being filtered and passed to a PDP 11/40 computer. Here the signals are digitized and Fourier transformed. The use of two quadrature signals improves the signal : noise ratio by $\sqrt{2}$ and enables the upper and lower side bands to be treated independently by means of the full complex transform, but the phase adjustment must be exact to avoid aliasing.

(*d*) *Resolving power*

The limiting factor controlling spatial resolution is the signal/noise ratio in the two signals, S_A and S_B. This ratio is directly proportional to the effective cross-sectional area of the selected line (δy and δz), so that the better the spatial resolution, the worse becomes the resolution of the signals for proton density or relaxation time. For this reason, the maximum of one line per cm was chosen, which gives a minimum cross section of 1 cm^2 for the line image. This is governed by the choice of field gradients and the incremental frequency of the carrier wave of the 180° pulse.

However, the resolution along the line depends on the Fourier transform process and the filtering that is applied to the imaging data. As a result, it can be altered even after the patient has gone. Although the potential resolution along the line is better than 3 mm, it may not be practical to go below 1 cm, again beause of signal : noise considerations.

Within these limits, a spatial resolution volume element, $\delta x\, \delta y\, \delta z$, can be chosen, which then determines how well differences of proton density or differences of T_1 can be discerned.

Figure 6 shows the estimated relation between T_1 resolution and the volume element size. This is for one triple-pulse sequence per line, or for a 2 min scan. A 50% change in T_1 in the trunk can be resolved in a spatial element of 2 cm^3, which will resolve a 10% change of T_1 in the head. Resolution can be improved by repeating the triple-pulse sequence N times and averaging the signals, thereby improving signal : noise by $\sqrt{N}$; this can be used either to improve T_1 discrimination or to distinguish between the same T_1 difference but with a smaller volume element (finer spatial resolution). A 50% change in T_1 in the trunk is therefore expected to be resolved with a volume element of about 0.5 cm^3 for a 30 min scan (15 triple-pulse sequences per line).

Figure 4 shows that the sensitivity to a given fractional change in T_1 is not independent of T_1,

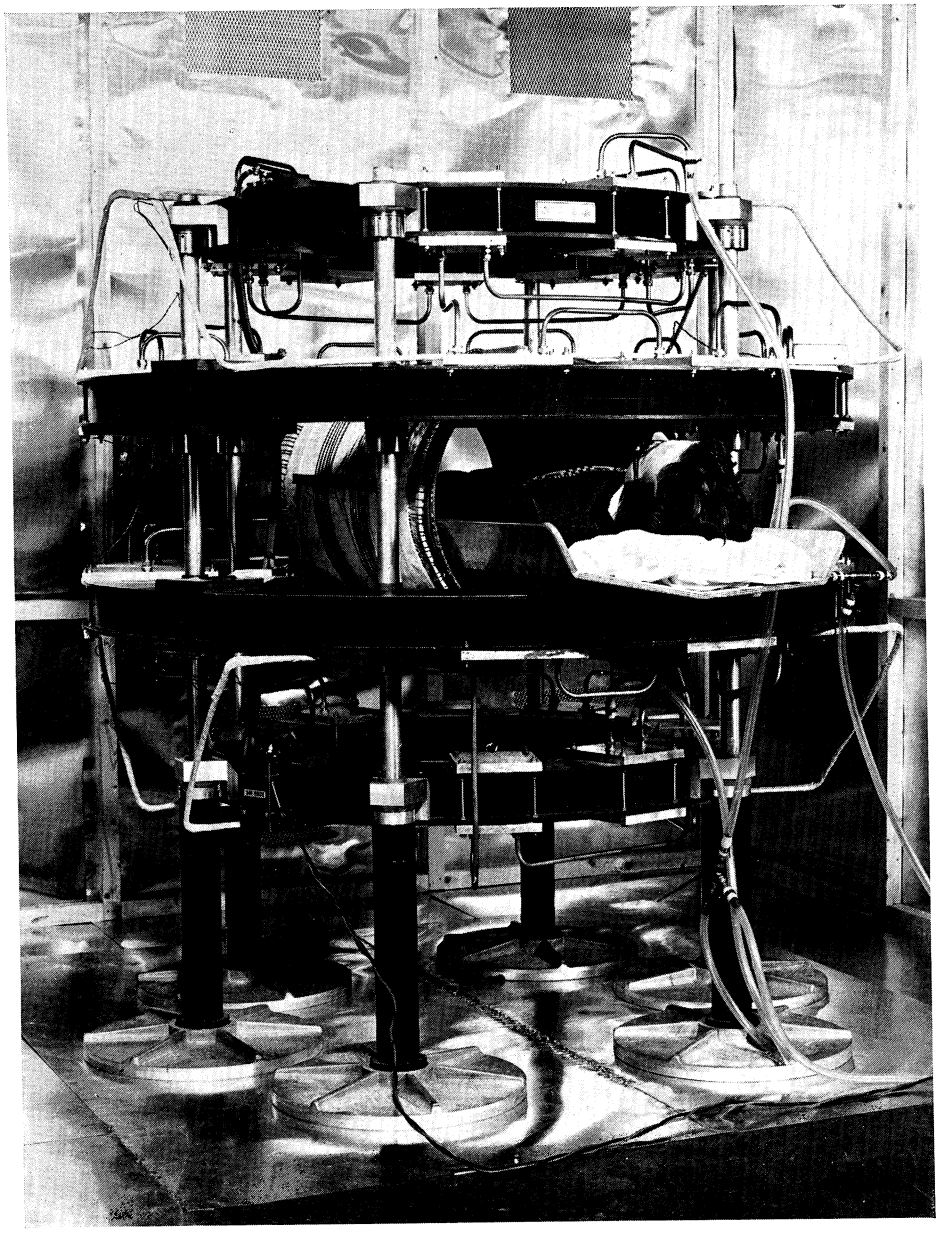

FIGURE 5. The Aberdeen n.m.r. imaging machine (January 1979).

(*Facing p.* 524)

PHILOSOPHICAL TRANSACTIONS OF THE ROYAL SOCIETY B BIOLOGICAL SCIENCES

but has a broad maximum in the region of 200 ms; this was chosen to coincide with the measured range of T_1 values (see § 4.)

Improvement in resolution can be sought. The number of image lines can be increased by increasing G_z (and probably a flatter waveform); δy could be reduced by increasing G_y. Such gains lead to a loss of signal:noise ratio, which, in general, is related to (frequency)$^{\frac{3}{2}}$ and hence (magnetic field)$^{\frac{3}{2}}$. To halve the linear resolution (i.e. volume element reduced to one-eighth) leads, therefore, to the need for a fourfold rise in the magnetic field strength, which in turn requires a new magnet design. Other marginal gains might also be possible.

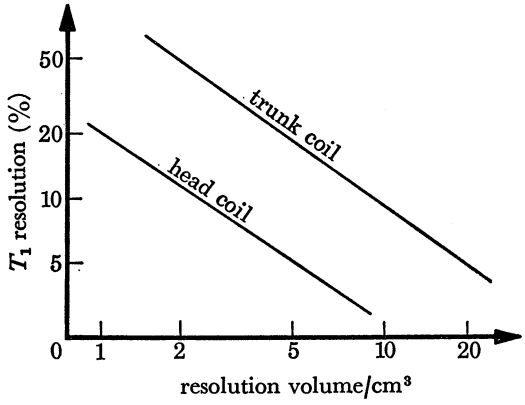

FIGURE 6. The predicted relation between the spatial resolution (the elemental volume size) and T_1 resolution for one pulse sequence per line for both a large r.f. coil (trunk imaging) and a smaller one (head imaging).

4. *IN VITRO* MEASUREMENT OF SPIN–LATTICE RELAXATION TIME (T_1)

(*a*) *Normal tissues*

The human body is extremely complex. When trying to image a new property such as n.m.r. relaxation, this very complexity makes it difficult to interpret the results. This is especially true if n.m.r. images are compared with images obtained from other tissue properties, e.g. X-ray absorption, radiopharmaceutical concentration, or ultrasound characteristic impedance.

It is with this in mind that we are approaching the interpretation of the n.m.r. images by direct comparison, where possible, with quantitative results from *in vitro* tissue studies (Mallard *et al.* 1979). The Aberdeen imaging system is capable of selectively imaging proton (water) concentration or T_1 relaxation and, therefore, *in vitro* studies of T_1 are of direct relevance. Also, the considerable range of T_1 values for the different soft tissues suggests that the resolution of images based on these measurements may be better than that achieved if the very small differences in water content between the soft tissues are imaged alone.

Most of the *in vitro* experiments have been carried out at 24 MHz with samples of about 0.2 cm^3 in volume. This is an ideal sample size for looking at T_1 relaxation values of small tissues such as nerves and gives a better measurement for larger tissues. This is because the small amounts required allow different regions of an inhomogeneous tissue to be examined separately, so avoiding mixed tissue samples, which would appear as a nonlinearity in the exponential relaxation.

For tissues from which sufficient material was available, we have been able to carry out additional measurements of T_1 values at 2.5 MHz. The results have indicated that T_1 values at

PHILOSOPHICAL TRANSACTIONS OF THE ROYAL SOCIETY B BIOLOGICAL SCIENCES

the lower frequency are about one half of those at the higher one. This gives some confidence in the use of the *in vitro* results obtained at 24 MHz to predict the ratios between T_1 values of different tissues at the operating frequency of the present imaging machine (1.7 MHz).

TABLE 1. COMPARISON OF T_1 RELAXATION TIMES OF SKIN, LIVER AND SPLEEN BETWEEN DIFFERENT MAMMALIAN SPECIES (after Mallard *et al.* 1979)

(measured at 24 MHz; ± standard deviation)

	T_1/ms		
	liver	spleen	skin
human	339 ± 42	535 ± 116	471 ± 40
rat	324 ± 12	531 ± 64	400 ± 37
rabbit	309 ± 35	529 ± 46	430 ± 80

TABLE 2. SPIN–LATTICE RELAXATION TIME (T_1) OF NORMAL TISSUES OF THE RABBIT, MEASURED AT 24 MHz (Mallard *et al.* 1979)

(T_1 for free water = 3.5 s.)

T_1/ms	tissues within this range
150–250	mesentery, skull bone, rib, bone marrow
250–350	trachea, colon, ureter, skeletal nerve, pancreas, heart edge of liver
350–450	main part of liver, wall of small intestine, stomach wall, salivary gland, adrenal gland
450–550	aorta wall, thyroid, carotid wall, kidney cortex, medulla oblongata, spleen, skeletal muscle, white brain
550–650	rectum wall, bladder wall, rectus abdominus, intercostal muscle, epidydimis
650–750	diaphragm, cerebellum, auricle, ventricle, upper lung, grey brain
750–850	lower lung, testis, kidney medulla, whole blood

Rats and rabbits have provided a ready source of material for these measurements. Comparison of values for T_1 of skin, liver and spleen in rats, rabbits and humans (table 1) shows that there is considerable similarity between these species. On this basis we have used small mammals in large-scale experiments to map the range of T_1 values of normal tissue (Mallard *et al.* 1979). The size of the rabbit has made it useful for such studies. Over 50 different tissues from each rabbit have been examined, including small tissues such as lymph nodes and trunk nerves. Values of T_1 range from 166 ± 20 ms for mesentery and 172 ± 15 ms for white bone marrow, to 831 ± 39 ms for kidney medulla and 868 ± 45 ms for heparinized whole blood (table 2). These have been drawn on an anatomical map of the rabbit to illustrate the spatial distribution of the various T_1 values in the body (figure 7, plate 2).

Ultimately, the whole body n.m.r. imaging machine is for human work, but there are many problems in producing maps of *in vitro* results from human material. The only time when a wide range of normal tissues can be obtained from a single human being is at post-mortem examination. However, such material is available, at the earliest, 24 h after death, by which time degenerative changes have started in the tissue. For rat tissues, we have found that, if samples are stored, T_1 values generally decrease with time after death. The change in T_1 for different tissues is very variable and a change of storage conditions, such as temperature, can cause considerable differences. Chang *et al.* (1976) have measured T_1 relaxation for long decay periods and have found multi-components; the relation between the short and long components of the relaxation time was very variable during the first 6 h after death. Similar results have been

PHILOSOPHICAL TRANSACTIONS OF THE ROYAL SOCIETY B BIOLOGICAL SCIENCES

found by Sandhu & Friedman (1978), working with the tails of newts, and Barroilhet & Moran (1975), using mice. We have made some measurements on rat muscle samples and found similar complications in the relaxation time values. It is for these reasons that human post-mortem material has not been used in this study for the detailed mapping of T_1 values of the normal tissues.

(b) Pathological tissues

Many groups have measured the relaxation time of water protons in tumours. Results have indicated that malignant tissues generally have longer relaxation times than the equivalent normal tissues (Damadian *et al.* 1973; Hollis *et al.* 1973), although it is now recognized that there is considerable overlap of values (Eggleston *et al.* 1975; Koutcher *et al.* 1978). Results in our laboratory with tumours (Gordon *et al.* 1978) have been in accord with those of most other workers. Also, more recent small-scale studies have shown that freshly excised human breast tumours have T_1 values of over 550 ms, compared with a T_1 value of less than 250 ms for the surrounding tissue (table 3), but the latter has a multiple-component relaxation, which is always found in fatty tissue. Post-mortem study in two instances with metastatic tumour in the liver has shown T_1 values of 650–800 ms for metastatic tissue, as compared with the value of 340 ± 42 ms for normal human liver (table 3).

TABLE 3. COMPARISON OF T_1 RELAXATION TIMES (AT 24 MHz) OF FRESHLY EXCISED HUMAN BREAST TUMOURS WITH SURROUNDING HOST TISSUE AND OF POST-MORTEM SAMPLES OF LIVER METASTASES WITH NORMAL LIVER TISSUE (Mallard *et al.* 1979)

breast tumours	$T_1 > 550$ ms, single exponential
host tissue	$T_1 < 250$ ms, multiple exponential (characteristic of fatty tissue)
Expected linear spatial resolution $\approx$ 7 mm (half hour scan).	
tumour metastases in liver	$T_1 = 650$–800 ms
host tissue	$T_1 = 300$ ms (rather less than normal liver at 340 ms)
Expected linear spatial resolution $\approx$ 7 mm (half hour scan). N.B. Fluid filled cysts expected to give finer resolution.	

We have found that undifferentiated transplantable animal tumours have long T_1 values, e.g. Yoshida sarcoma has a T_1 value of about 780 ms. Such a tumour has been used to study problems associated with the sharpness of imaging the tumour margin, which is of clinical importance (Ling *et al.* 1979).

The spatial resolving power of the imaging technique itself will lead to degradation of the sharpness of the margin, and it was wondered how this would be affected by biological processes such as inflammation, local immune reactions and invasion of neighbouring tissue by the tumour. We have examined this in rat muscle by means of Yoshida sarcoma implanted subcutaneously in the upper thigh (figure 8*b*, plate 1). The reaction of the underlying muscle was observed during the first ten days after implantation by taking a strip of this tissue from the centre of the tumour, outwards to well away from the tumour growth itself (figure 8*a*).

The muscle immediately adjacent to the tumour shows an increased T_1 value within two days of implantation, and we believe that this is largely due to inflammatory and local immunological reactions in the tissue. As one progresses outwards further than about $\frac{1}{2}$ cm from the edge of the tumour, the T_1 value decreases to normal (figure 8). The normal T_1 value for each rat is ascertained by taking a piece of muscle from the opposite thigh (Ling *et al.* 1979).

5. Discussion of the potential clinical value of the n.m.r. imaging technique

The highest T_1 values for normal tissue are over five times the lowest T_1 values. This range is considerably greater than the range of water concentration values for soft human tissues, which vary from 69% for skin, through 79% for skeletal muscle, spleen and lung, to 83% for grey brain tissue (72% white brain tissue). This suggests that the discrimination and spatial resolution of some soft tissues may be better on T_1 images than on proton concentration images. In addition, the range of T_1 values for soft tissues to be imaged is much greater than the variation of other properties used in the many different methods of medical imaging, e.g. X-rays, radionuclides, ultrasound. This seems a good augury for the clinical usefulness of n.m.r. imaging. The difference of T_1 values to be expected for different organs may give an unique identification of the organ in addition to its position and shape (see figure 7).

Many adjacent soft tissues show very different T_1 values. For example, at 24 MHz the T_1 value of the kidney medulla is about 800 ms, while that of the kidney cortex is about 500 ms. Similarly, the T_1 value of grey brain tissue is about 700 ms, while that of the white brain tissue is about 500 ms. These adjacent tissues may, therefore, be distinguishable by the n.m.r. imaging process.

The increased value for T_1 found in tumours has led to much speculation that n.m.r. imaging will prove valuable for their detection. However, it must be borne in mind that other imaging techniques exist that are very effective for this purpose, each with their own particular site or tumour type for which they are eminently successful, e.g. X-ray or isotope c.a.t. scanning for brain tumours, isotope emission scanning for bone tumours. While the n.m.r. technique is unlikely to have the spatial resolution of X-ray c.a.t. scanning, it may have a resolution closer to that of the isotope procedure, but will image a different physiological function from it. It does seem, however, that there may be some particular merit in n.m.r. imaging for detecting breast tumours and liver metastases, as seen from table 3. As yet there are few signs that the technique will help in the important problem of discriminating between malignant and benign lesions.

The elevation of T_1 that has been found in normal tissue around a tumour (see figure 8) will have the effect of enhancing the image degradation of the edge of such a tumour and will decrease the resolution of the tumour image. This effect may be even worse in tumours where there is dendritic invasion into surrounding tissues. However, one of the main objects of the diagnostic exercise is to find small tumours, and the tissue reaction to the tumour may have the effect of making it appear larger, which may, in turn, lead to the earlier detection of tumours.

It is very important to realize that many conditions other than malignancy may change the T_1 of body tissues, for example, anything that gives rise to a change in water content of a tissue, either intracellular or extracellular. As a result, any condition that produces oedema should give rise to an increase in T_1 in the region affected, as should diseases that produce abnormal fluid pools in the body, perhaps, for example, from bronchial asthma, pleural effusions, fluid-filled cysts, ulceration, abnormal synovial fluid volume in joints, arthritis and so on.

It may also be possible to detect degenerative nerve changes; e.g., Go & Edzes (1975) have used the chemical triethyl tin to induce brain oedema, and have found increased T_1 relaxation times in white brain matter, which they attribute to vacuolation of the myelin sheath of the nerve fibres.

PHILOSOPHICAL TRANSACTIONS OF THE ROYAL SOCIETY B BIOLOGICAL SCIENCES

Plaque and thrombus formation in the aorta may be detectable by nuclear magnetic resonance. In rabbits, the T_1 value of the aortic arch is 425 ms, while that of clotted blood is about 650 ms, both measured at 24 MHz, but the rhythmical movement of the vessel will prove a disturbing factor.

Recent suggestions include the possibility of finding early ascites before it becomes clinically detectable, glaucoma and Meniere's disease, nephrotic syndrome, Alzheimer's disease, hydrocephalus and pre-menstrual tension, and even an investigation as to whether 'hangover' the morning after the night before, is accompanied by dehydration or over hydration!

6. Potential hazards to the patient

The three aspects of n.m.r. imaging that may lead to potential hazards for the patient are r.f. heating, the static magnetic field and the induction of electric currents in the body due to rapid changes in the magnetic field. There is an extensive literature on such effects (see, for example, Barnothy 1964, 1969; Persinger 1974), but there is a dearth of properly documented, carefully controlled experiments.

The heating effect from r.f. fields has led to health standards (see Budinger 1979) being laid down on the concept that it should not exceed the basal metabolic rate, which is approximately 1 W/kg. The level in the Aberdeen machine is only 100 mW for the total body (i.e. 70 kg).

Budinger (1979) has reviewed physiological effects of static magnetic fields and concludes that fields up to 0.5 T should be tolerated without ill effects but that cardiac electro-physiological phenomena should be investigated further in fields above 0.3 T (the Aberdeen field strength is 0.04 T). Also, he concludes that time-varying fields with $\mathrm{d}B/\mathrm{d}t$ of 3 T/s should not cause biological effects. The wave form, energy and repetition rates are important parameters, particularly if field changes greater than 3 T/s are required. In the Aberdeen system, the peak rate of change of field is during the G_y pulse, and just reaches 3 T/s near the ends of the patient tube. However, the duty cycle is only 0.2% and none of the volunteers have reported any subjective effects.

7. Early images from the whole body machine

At the time of writing the machine is incomplete, but some early images are shown here. Figure 9*a*, plate 1, shows the image of a square array of identical bottles of copper sulphate solution. The skewness is probably caused by magnetic field gradients not being perfectly aligned. Figure 9*b* is the image of two boxes of copper sulphate solution, the left hand one having twice the T_1 value of the other. The T_1 image profile (bottom) shows the T_1 discrimination, displayed also by the colour coding of the image. Figure 10, plate 1, is our first human image, which is a section through the thorax of one of us (J.M.S.H.). The lungs, heart and spine can be seen, of recognizable shape and size. The bar across and beyond the trunk section is a movement artefact caused by heart beats, one of many problems yet to be overcome.

The *in vivo* images need much improvement to become acceptable. Since a genuine clinical role has yet to be found and since the machines are expensive to build, it will be some considerable time before a commercial version becomes viable to make them more generally available for wider exploration and use. However, this period may be exciting and valuable.

PHILOSOPHICAL TRANSACTIONS OF THE ROYAL SOCIETY B BIOLOGICAL SCIENCES

References (Mallard *et al.*)

Barnothy, M. F. (ed.) 1964, 1969 *Biological effects of magnetic fields*, vols 1 and 2. New York: Plenum Press.
Barroilhet, L. E. & Moran, P. R. 1975 *Med. Phys.* **2**, 191–194.
Budinger, T. F. 1979 *Proc. Workshop on computerized tomography (Irvine, California). IEEE Trans. nucl. Sci., new Series* **26**, 2821–2825.
Chang, D. C., Hazlewood, C. F. & Woessner, D. E. 1976 *Biochim. biophys. Acta* **437**, 253–258.
Damadian, R., Zaner, K., Hor, D., DiMaio, T., Minkoff, L. & Goldsmith, M. 1973 *Ann. N.Y. Acad. Sci.* **222**, 1048–1078.
Eggleston, J. C., Saryan, L. A. & Hollis, D. P. 1975 *Cancer Res.* **35**, 1326–1332.
Go, K. G. & Edzes, H. T. 1975 *Arch. Neurol., Chicago* **32**, 462–465.
Gordon, R. E., Mallard, J. R. & Philip, J. F. 1978 In *Nuclear magnetic resonance effect in cancer* (ed. R. Damadian), ch. 16. Portland, Oregon: Pacific Publishing Co.
Hollis, D. P., Economou, J. S., Parks, L. C., Eggleston, J. C., Saryan, L. A. & Czeisler, J. L. 1973 *Cancer Res.* **33**, 2156–2160.
Hutchison, J. M. S., Mallard, J. R. & Goll, C. C. 1974 *Proc. 18th Ampere Congress (Nottingham)* (ed. P. S. Allen, E. R. Andrew & C. A. Bates), pp. 283–284. University of Nottingham.
Hutchison, J. M. S. 1976 *Proc. 7th L. H. Gray Conference, Medical Images (Leeds)*, pp. 135–141. Bristol: Wiley/Institute of Physics.
Hutchison, J. M. S. 1979 *IEE med. Electron. Monogr.*, nos 28–33 (ed. B. W. Watson), pp. 79–93. London: Peter Peregrinus.
Hutchison, J. M. S., Sutherland, R. J. & Mallard, J. R. 1978 *J. Phys.* E **11**, 217–221.
Koutcher, J. A., Goldsmith, M. & Damadian, R. 1978 *Cancer* **41**, 174–182.
Ling, C. R., Foster, M. A., & Mallard, J. R. 1979 *Br. J. Cancer* **40**, 898–902.
Mallard, J. R. 1979 Nuclear imaging. In *Electronic imaging* (ed. T. P. McLean & P. Schagen), pp. 415–459. London: Academic Press.
Mallard, J. R., Hutchison, J. M. S., Edelstein, W., Ling, C. R. & Foster, M. A. 1979 *J. Bio-Med. Engng* **1**, 153–168.
Persinger, M. A. (ed.) 1974 *E.l.f. and v.l.f. electromagnet field effects*. New York: Plenum Press.
Sandhu, H. S. & Friedmann, G. B. 1978 *Med. Phys.* **5**, 514–517.
Sutherland, R. J. & Hutchison, J. M. S. 1978 *J. Phys.* E **11**, 79–83.

Discussion

S. F. J. Cox (*Rutherford Laboratory, Chilton, Didcot OX*11 0*QX, Oxfordshire, U.K.*). A number of speakers have mentioned that the n.m.r. signal detected in imaging will depend on liquid flow rate. The basis for this is that if an average r.f. power is used that is sufficient to partially saturate the nuclear resonance in the static liquid, introduction of fresh liquid into the sensitive region will reduce the degree of saturation. May I ask if there are any groups trying to exploit this principle and whether on a large scale we may hope to display regions where the blood flow is perturbed (by a stroke or blood clot for instance), or on a smaller scale to display the flow profile within a single vessel?

P. C. Lauterbur. We have used the sensitive point method to scan pulsatile flow in a phantom, a simulated artery, with use of the fact that the n.m.r. response is a function of flow velocity.

P. Mansfield. We have made mathematical simulations of the effect of flow on the spin image and predict that 'vectorial flow' (i.e. direction as well as rate) can be displayed. We propose to use the pulsatile nature of blood flow to subtract its signal from the static background and hope to plot the velocity profile within the aorta. In addition, our imaging speeds are now such that we can hope soon for 'real time' imaging, displaying other bodily motions such as breathing.

J. Mallard. I am most interested in Dr Mansfield's observations, because, it seems to me, that the n.m.r. thorax cross section, taken on the Aberdeen machine, that was shown, was spoilt by

PHILOSOPHICAL TRANSACTIONS OF THE ROYAL SOCIETY B BIOLOGICAL SCIENCES

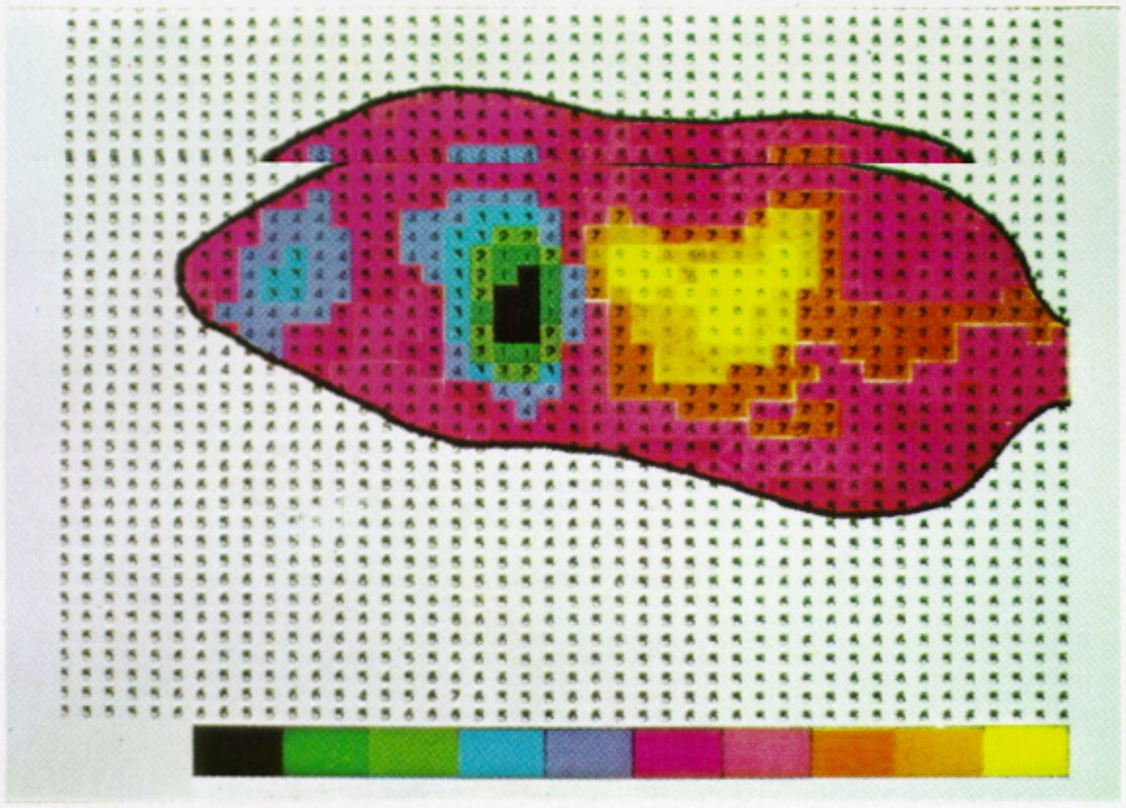

1

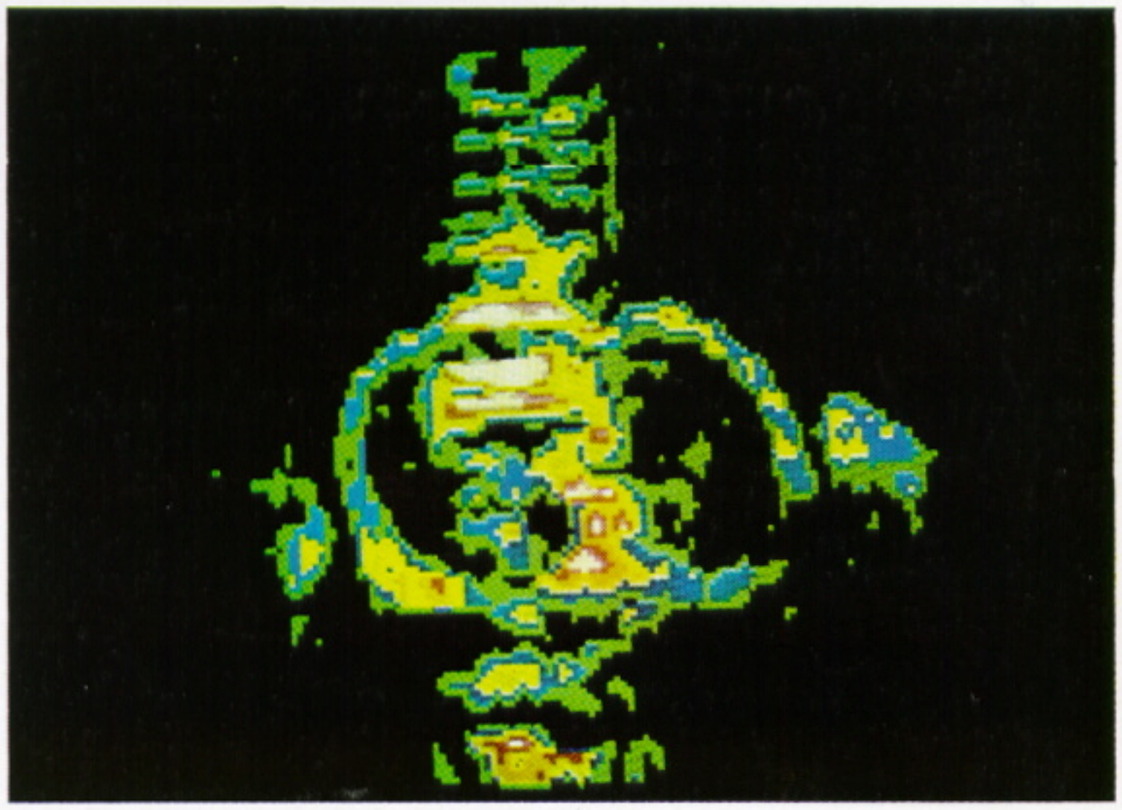

10

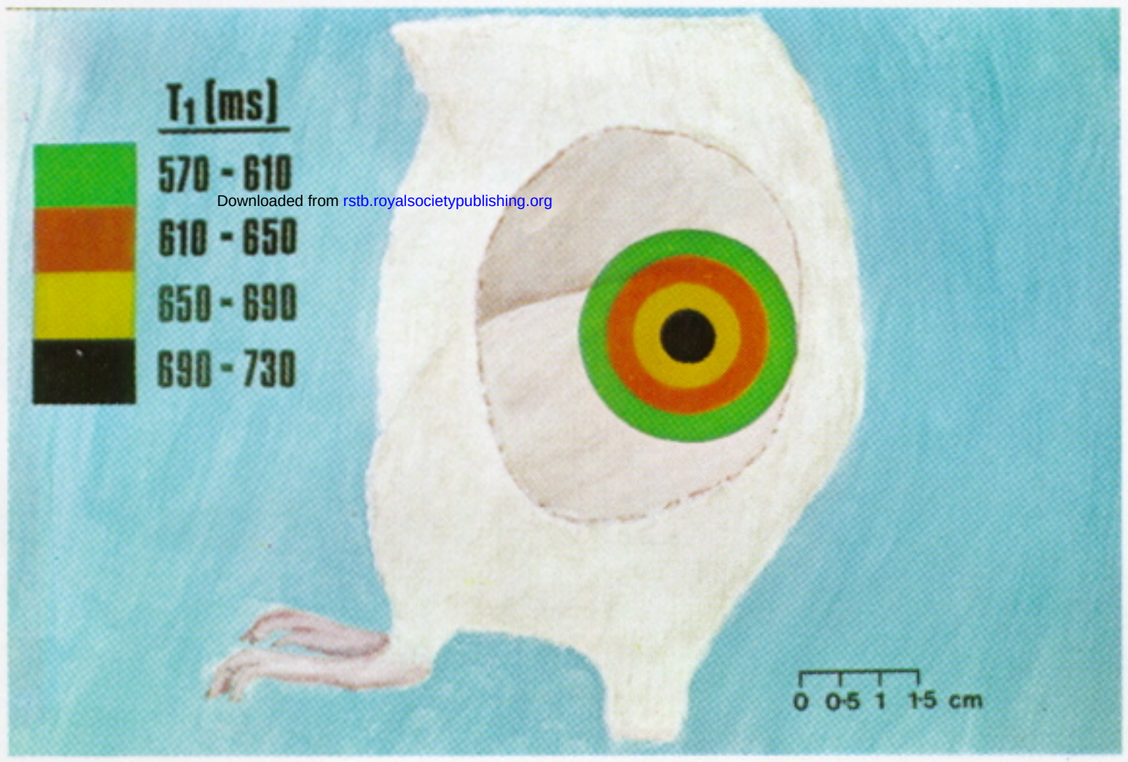

8a

8b

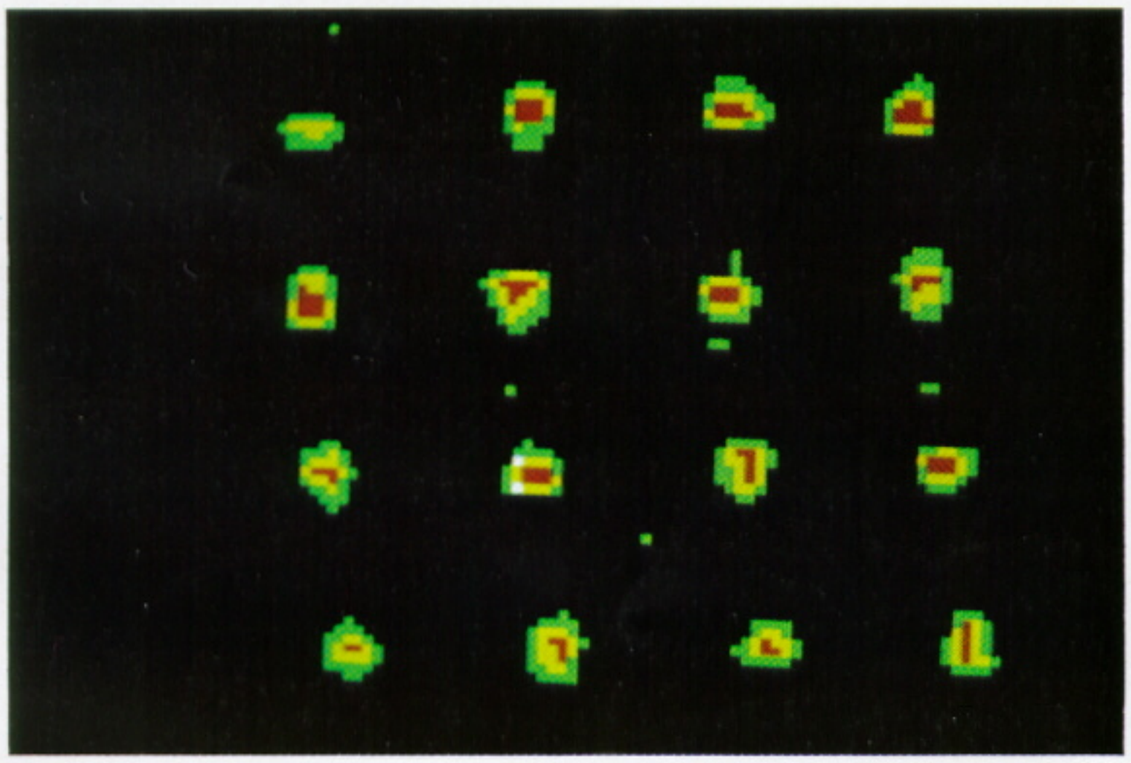

9a

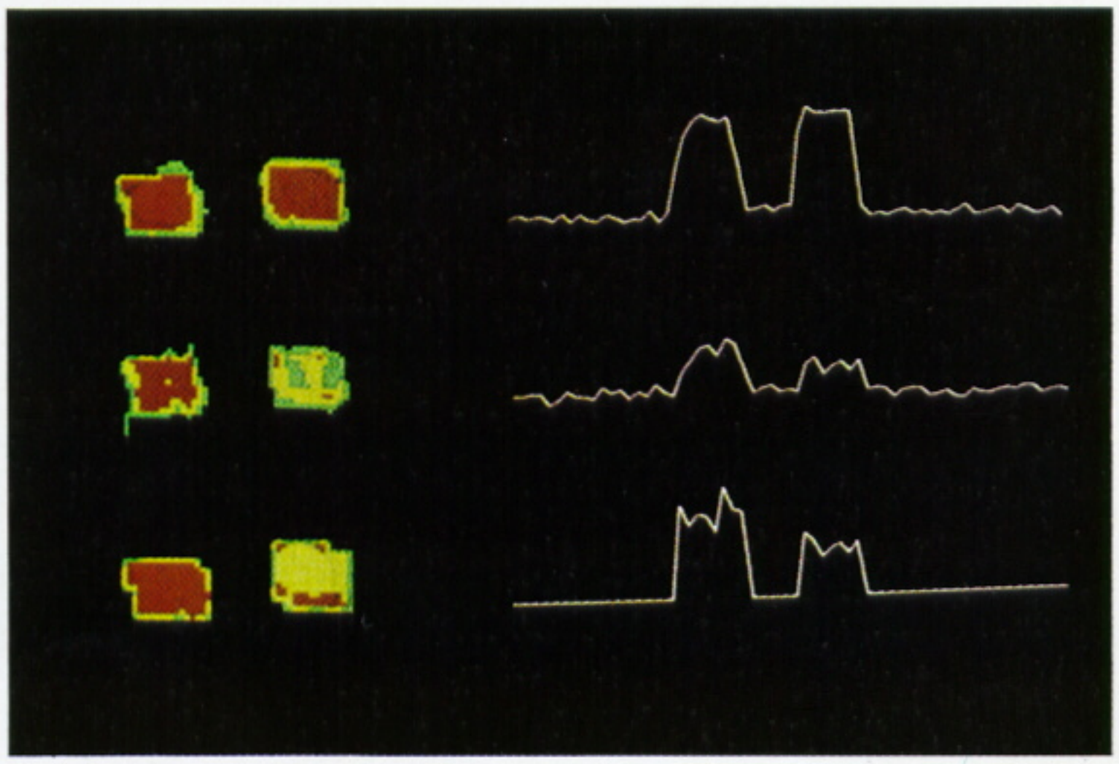

9b

FIGURES 1, 8–10. For description see opposite.

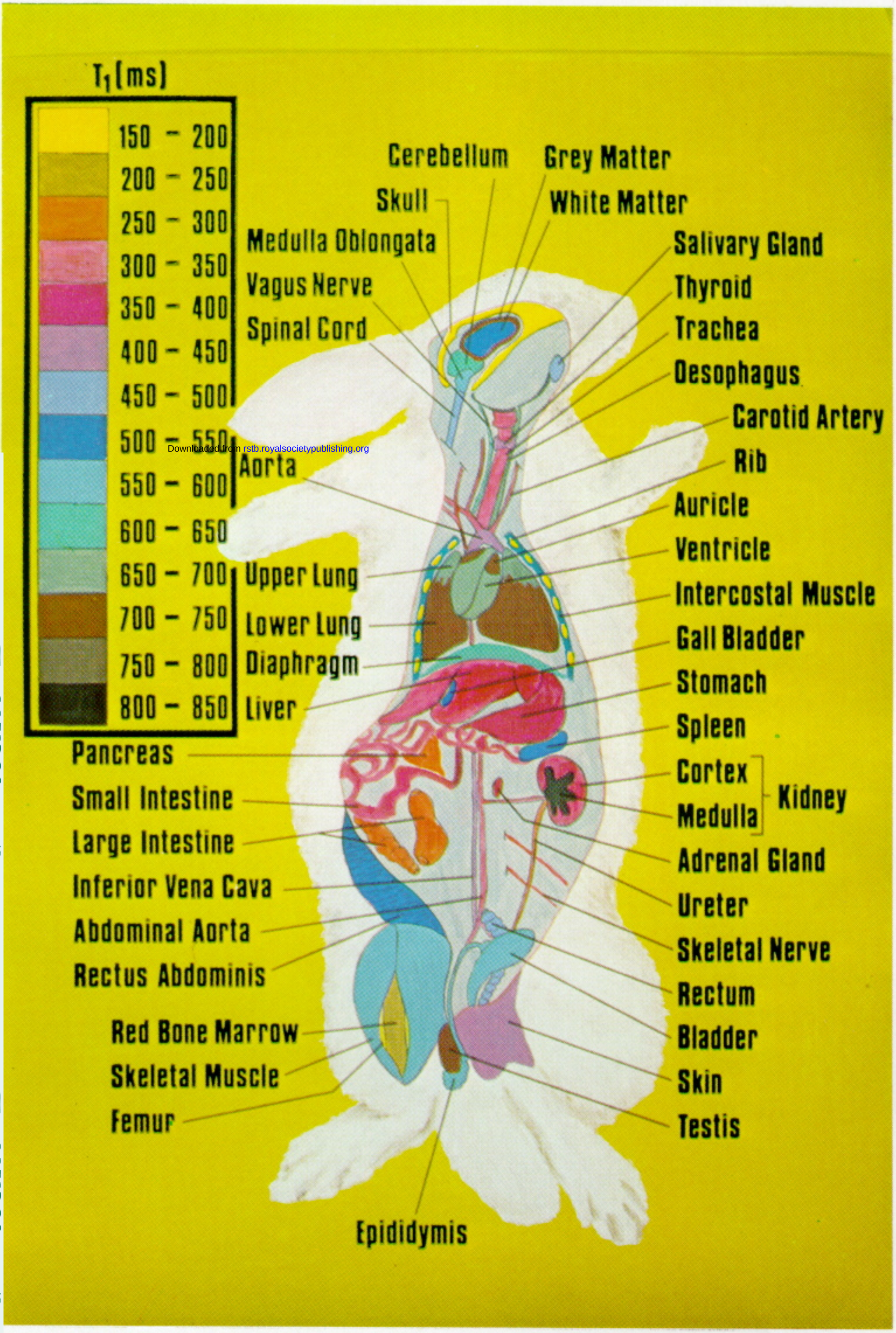

PHILOSOPHICAL TRANSACTIONS OF THE ROYAL SOCIETY B BIOLOGICAL SCIENCES

FIGURE 7. For description see opposite.

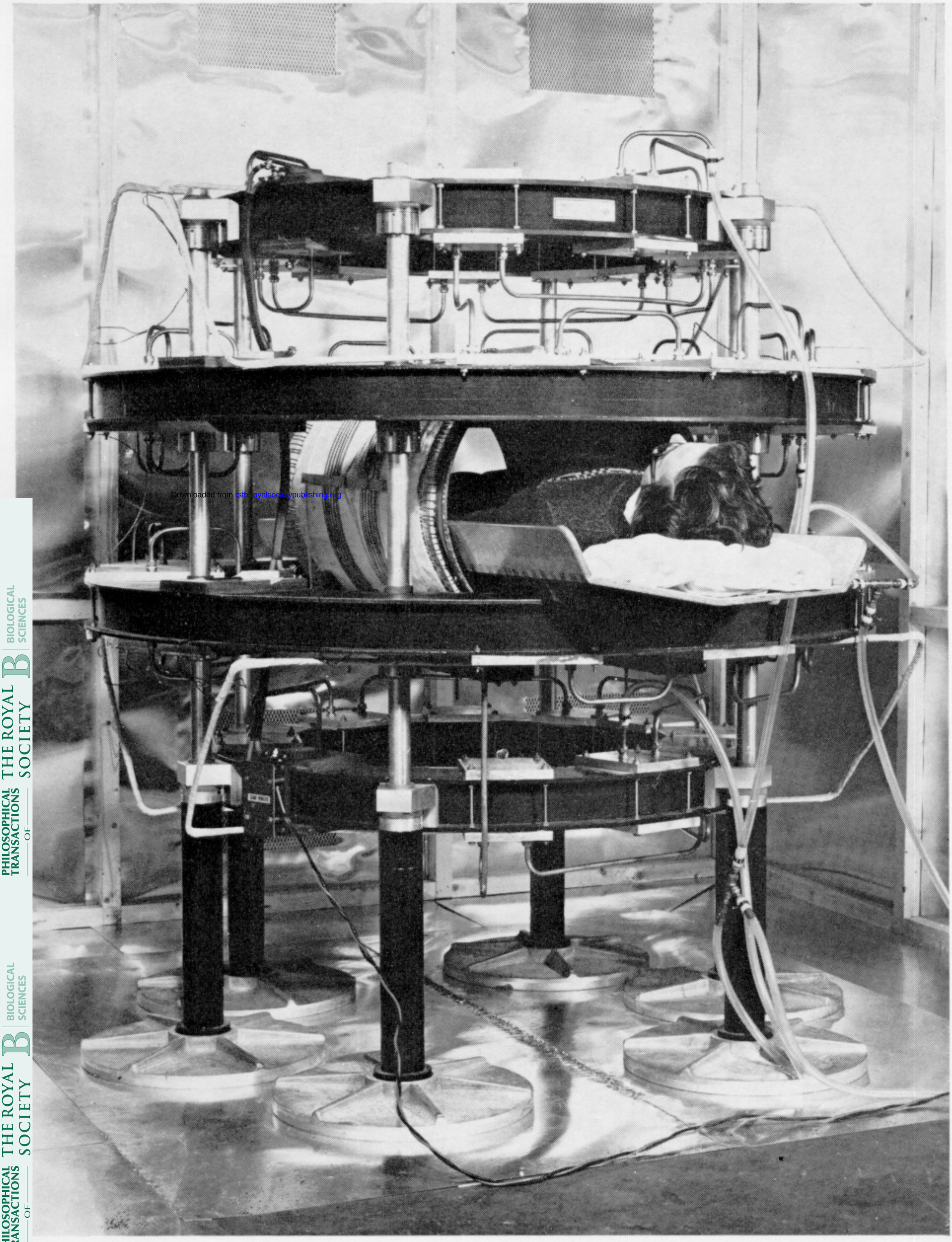

FIGURE 5. The Aberdeen n.m.r. imaging machine (January 1979).